How a Transition State Tightens: The Singlet Photodissociation of Ketene as a Test Case

Elisabeth A. Wade,† Axel Mellinger, Melonie A. Hall, and C. Bradley Moore*

Chemical Sciences Division, Lawrence Berkeley National Laboratory, Berkeley, California 94720, and Department of Chemistry, University of California, Berkeley, California 94720-1460

Received: February 28, 1997; In Final Form: May 5, 1997[⊗]

The tightening of the transition state as energy increases above the dissociation threshold is studied for the dissociation of singlet ketene. Rate constants and quantum yields have been determined for the photodissociation of ketene to produce $CH_2(\tilde{a}^1A_1)(0,0,0) + CO(\tilde{X}\ ^1\Sigma^+)(v=1)$. At 57, 110, 200, 357, and 490 cm^{-1} above this threshold, vibrational branching ratios for the singlet products were measured and compared to theory. Above 100 cm^{-1}, the experimental values are consistent with the separate statistical ensembles (SSE) and variational RRKM models. $CO(v=1,J)$ photofragment excitation (PHOFEX) spectra were observed up to 300 cm^{-1} over the threshold for production of $CO(v=1)$ and used to calculate the total yield of the state probed. The J dependence of these yields is statistical, consistent with the observed $^1CH_2$ rotational distributions. Thus, the total $CO(v=1)$ singlet yield and rate constant are determined as a continuous function of energy up to 300 cm^{-1}. Rate constants are given accurately by phase space theory (PST) up to 35 ± 5 cm^{-1}. The *ab initio* rate constants of Klippenstein, East, and Allen match the experimental rate constants from 10 to 6000 cm^{-1} well within experimental uncertainty without any adjustment of parameters for the unified statistical model of Miller. Thus the rate appears to be controlled by an inner transition state near 3 Å and the outer PST transition state acting in series with the outer transition state dominating for energies below 50 cm^{-1} and the inner for energies above a few hundred cm^{-1}. From the measured rate constants, an experimental density of states is calculated to be 0.94 times the anharmonic *ab initio* density of states. This allows the degeneracy g_t of the coupled triplet channels to be determined from the rates at the triplet threshold, $g_t = 1.0 \pm 0.1$. The vibrational branching ratios and product yields for the vibrationally excited triplet products were also estimated and found to be nearly constant over this energy region. These values are about 17% of those predicted for vibrationally adiabatic dynamics in the exit valley after passage through the triplet transition state.

I. Introduction

For unimolecular reactions controlled by a transition state at the top of a barrier between reactant and products, Rice−Ramsperger−Kassel−Marcus (RRKM) theory can provide quantitative predictions of the rate.[1−5] In the absence of a barrier to recombination of product fragments, it is more difficult to define and locate a transition state on the potential energy surface (PES) for the reaction and there has been considerable theoretical work on models for such reactions.[1,5−23]

At the energetic threshold for unimolecular reactions without a barrier to recombination on the surface for zero point vibrational energy, the rate is limited only by the number of available product states, the phase space theory (PST) limit.[7,24,25] The sum of states or open reaction channels, $W_{PST}(E,J)$, is easily calculated from the energy levels of the products. This sum may then be used in the statistical transition state theory expression for the rate constant[1,5]

$$k(E,J) = W(E,J)/h\rho(E,J) \qquad (1)$$

where E is the total energy and J is the total angular momentum quantum number of the reactant molecule. The density of states, $\rho(E,J)$, is estimated from the spectroscopy of the stable molecule or directly measured spectroscopically.[3,5,25,26] Exactly at threshold, there is only one energetically accessible channel, and PST must, by definition, provide the correct statistical rate constant. The product energy state distributions for NCNO[27,28] and CH_2CO,[24,29−32] and indirect measurements of rate constants for CH_2CO[33] and NO_2,[25,26] are consistent with PST predictions near the energetic threshold. Well above threshold, PST seriously overestimates rate constants.[5]

As the fragments approach each other along the reaction coordinate, a bond begins to form, rotations become hindered, and energy level spacings increase. The number of open channels $W(E,J,R)$ varies along the reaction coordinate, R (Figure 1). In variational RRKM (var. RRKM) theory,[8−14] the minimum value of $W(E,J,R)$ at $R^{\ddagger}(E,J)$ defines $W(E,J)$ and the location of the transition state along the reaction coordinate. In the statistical adiabatic channel model (SACM),[15,16] the energy states are correlated to define adiabatic channel potentials along R. A channel is counted in $W(E,J)$ if its maximum is below E for the given value of J. In both var. RRKM and SACM, the transition state moves inward along the reaction coordinate with increasing energy. These two models are identical to PST at threshold and give rate constants which increase less rapidly with energy than do PST rate constants. Additionally, while SACM and var. RRKM are based on different hypotheses, they give identical rate constants when used with identical sets of noncrossing adiabatic channel curves.[3]

$W(E,J,R)$ may not vary monotonically with R. *Ab initio* calculations by Katagiri and Kato for NO_2 show that channel maxima move in from the PST limit directly to an NO distance of 3.2 Å within 5 cm^{-1} of threshold.[17] Calculations on CH_2CO exhibit this same sudden tightening to 3.2 Å at about 140 cm^{-1}.[13] Thus, there are two minima in $W(E,J,R)$, $W_{PST}(E,J)$ and $W_{inner}(E,J)$, with a maximum $W_{max}(E, J)$ at an intermediate value of R. The smaller of the two minima is used in eq 1 in

† Current address: Department of Chemistry, San Jose State University, San Jose, CA 95192-0101.

[⊗] Abstract published in *Advance ACS Abstracts,* August 1, 1997.

S1089-5639(97)00765-2 CCC: $14.00

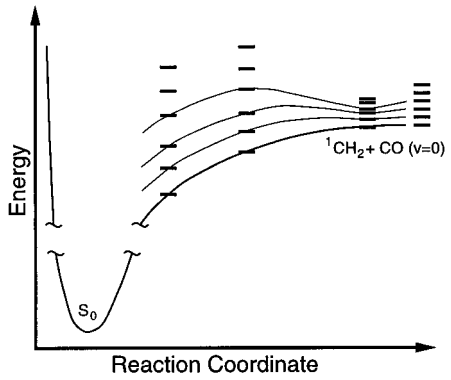

Figure 1. Schematic diagram for dissociation on a vibrationally adiabatic potential energy surface. As the chemical bond tightens, the level spacings increase. For var. RRKM, the transition state occurs at the product fragment separation for which the number of states is at its minimum. This causes the transition state to move in along the reaction coordinate as energy increases. Similarly, for SACM, each final state (e.g., $CO(v=0,J=5) + {}^1CH_2(J_{K_aK_c}=4_{14})$) is correlated along the reaction coordinate to give rovibrational adiabatic channels with barriers that move in along the reaction coordinate. For both SACM and var. RRKM, $W(E,J)$ becomes smaller at this tight transition state than at the free-rotor asymptote considered in PST as energy increases above threshold.

standard var. RRKM. Miller's unified statistical model[18,19] shows that if energy randomizes between these two bottlenecks (i.e., dynamics are completely non-adiabatic and all channels open at this intermediate value of R are randomly sampled), they may both act as transition states. This provides a physical model corresponding to the multiple reflections of reactive flux proposed by Hirschfelder and Wigner.[34] In its simplest form this gives[19]

$$\frac{1}{W_{\text{eff}}(E,J)} = \frac{1}{W_{\text{inner}}(E,J)} + \frac{1}{W_{\text{PST}}(E,J)} - \frac{1}{W_{\text{max}}(E,J)} \quad (2)$$

Klippenstein and Marcus,[11] Klippenstein, East, and Allen,[13] and Klippenstein and Allen[14] have gotten better agreement between theory and many aspects of singlet ketene experiments with eq 2 than with the standard var. RRKM model. Near the reaction threshold a strongly attractive, isotropic long range potential can ensure that W_{max} is much larger than W_{inner} and W_{PST}; thus W_{max} can be neglected in eq 2. But even for this case, $W_{\text{max}}/W_{\text{PST}}$ must approach unity as the energy increases well above threshold as shown for NCNO in Figures 5 and 6 of ref 14.

Product vibrational degrees of freedom have been shown to evolve adiabatically from transition state to products for ketene as well as for NO_2 and NCNO.[3−5,10,11,30,31,33] For ketene, *ab initio* calculations show that the CO stretching frequency along the reaction coordinate is nearly equal to that for free CO.[13] Thus, for ketene $W(E,J)$ is the same function of energy above the threshold for each vibrationally excited product as for the ground state. These dynamics are incorporated into var. RRKM[10,11] as well as SACM[15,16] calculations. Product vibrational distributions can be understood quantitatively in terms of a model in which the transition state is defined separately for each vibrationally adiabatic potential leading to each combination of vibrational states of the fragments. Vibrational branching ratios are seriously underestimated by PST since at a given total energy the transition state for the vibrational ground state products is much tighter than that for vibrationally excited products. Var. RRKM calculations[10] predict the experimental branching ratios quantitatively with this vibrationally adiabatic model for both $^1CH_2$[31] and CO[33] produced by photodissociation of ketene.

The photodissociation of ketene provides a good test case for unimolecular reaction models. Ketene is excited by a UV pulse using a transition whose oscillator strength is derived from electronic excitation to the first excited state, S_1. Internal conversion to S_0 and intersystem crossing to T_1 provide strong coupling to these two potential energy surfaces from which dissociation occurs. Dissociation along the S_0 surface produces $CH_2(\tilde{a}\ ^1A_1) + CO(\tilde{X}^1\Sigma^+)$ ($^1CH_2 + CO$). There is no barrier to dissociation along this surface and there is only one electronic potential surface leading to these singlet products.[3] Indirect measurements[33] and var. RRKM calculations[12,13] of the singlet channel rate constant have suggested that the transition state is loose (PST) up to about 100 cm^{-1} over threshold. At higher energy, the experimental rate constant rises less rapidly than predicted by PST, which indicates that the transition state is tightening, consistent with var. RRKM and SACM.[9,35] However, the energy at which the transition state begins to tighten was not clearly established.

The primary goal of the present work is to observe the tightening of the transition state. Measurements of vibrational branching ratios and PHOFEX spectra for $CO(v=1)$ are combined with the previously determined singlet yield[32] and total rate constant data[35] for ketene photodissociation in order to determine the rate constant for singlet ketene dissociation to $CO(v=1)$ as a function of energy from 10 to 500 cm^{-1}. These rate data, the direct measurements from 450 to 6000 cm^{-1}, the vibrational branching ratios, and the PHOFEX spectra allow a clear choice among available models.

II. Experimental Section

Ketene was seeded in helium carrier gas, cooled by supersonic expansion into a vacuum chamber, and photolyzed with a pulse of tunable UV light (305−310 nm). The resulting CO was detected by laser-induced fluorescence (LIF) in the vacuum ultraviolet (VUV). Tunable VUV was generated either by frequency tripling in Xe or by resonant 2+1 sum-frequency generation in Mg/Kr, which is 20 times more efficient than nonresonant tripling. The VUV fluorescence was detected with a solar blind photomultiplier. The apparatus is as described in ref 32.

In a first set of experiments, vibrational branching ratios were measured at several energies up to 500 cm^{-1} over the threshold for production of $CO(v=1)$ by scanning the probe laser to collect spectra of the CO A ← X (3 ← 0) and (5 ← 1) bands at a fixed photolysis laser frequency. To minimize the effects of beam pointing instability resulting from scanning the dye laser, only a small portion of each $CO(v=0)$ and $CO(v=1)$ spectrum was collected. This portion of the spectrum contained at least 5 rotational lines, except at the lowest energies where there are fewer unoverlapped lines in the $CO(v=1)$ spectra in which case all resolved rotational lines were used. The experimental signal intensities are divided by the Franck−Condon and Hönl−London factors for the CO transition to obtain "reduced" intensities $S(v_{CO},J_{CO},h\nu)$. v_{CO} and J_{CO} are the vibrational and rotational quantum numbers of the CO photofragments, and $h\nu$ is the photon energy. The signal intensity $S(v_{CO},h\nu)$ for each vibrational state was then calculated as the measured line intensity $S(v_{CO},J_{CO},h\nu)$ divided by the experimentally determined fractional intensity for that rotational state taken from ref 32. $S(v_{CO},h\nu)$ was multiplied by the previously determined singlet yield to give $S_s(v_{CO},h\nu)$. The singlet channel vibrational branching ratio is then calculated as in ref 33. Each spectrum was recorded several times and checked for experimental drifts.

In the second series of experiments, the photolysis laser was scanned in steps of 0.5 cm^{-1} while the probe laser was set to a

TABLE 1: Vibrational Branching Ratios

excess energy (cm^{-1})[a]	$P_e(1\|s)/P_e(0\|s)$						$P_e(1\|t)/P_e(0\|t)$
	experimental[b]	PST	PST*[c]	SSE	var. RRKM[d]	prev exp	experimental[b]
57	0.0041 ± 0.0006	0.00066	0.0052	0.0034	0.0042		
110	0.0082 ± 0.0010	0.0021	0.016	0.0086	0.0095		0.074 ± 0.016
200	0.022 ± 0.004	0.0063	0.048	0.020	0.021		0.050 ± 0.006
357	0.044 ± 0.008	0.017	0.125	0.041	0.043	0.037 ± 0.010[e]	
490	0.070 ± 0.017	0.029	0.208	0.061	0.057		
570							0.044 ± 0.022

[a] Photon energy over the threshold (32 259.4 cm^{-1}) for production of CO(v=1) by the singlet channel. [b] 95% confidence intervals are given. [c] PST* uses the PST rate for CO(v=1) and the experimental data[35] for the total rate. [d] From ref 14. [e] From ref 33, multiplied by the singlet yield (ref 31).

single rovibrational transition of CO in order to collect photofragment excitation (PHOFEX) spectra. PHOFEX spectra were collected for the Q(3) and Q(7) lines for the first 300 cm^{-1} over the threshold for production of CO(v=1). PHOFEX spectra are reproducible to better than 10%.

III. Results

In a fully state-resolved experiment it would be possible to obtain completely state-resolved, microscopic rate constants $k_s(v_{CO},J_{CO},h\nu + E_i,J)$ and $k_t(v_{CO},J_{CO},h\nu + E_i,J)$ for the singlet and triplet channel, respectively, where J is the total angular momentum of the excited ketene molecule and E_i is the rotational energy of the ground state ketene prior to photoexcitation. The quantum yield for a particular rovibrational level of CO formed through the singlet channel is

$$\Phi_s(v_{CO},J_{CO},h\nu + E_i,J) = \frac{k_s(v_{CO},J_{CO},h\nu + E_i,J)}{\sum_{v_{CO},J_{CO}} k_s(v_{CO},J_{CO},h\nu + E_i,J) + \sum_{v_{CO},J_{CO}} k_t(v_{CO},J_{CO},h\nu + E_i,J)} \quad (3)$$

The analogous quantity for the triplet channel is defined by interchange of the s and t subscripts.

The experimental PHOFEX signal $S(v_{CO},J_{CO},h\nu)$ is not fully state-resolved. It is obtained by summing the product of the quantum yield and the absorption cross section $\sigma(h\nu,E_i)P(J,J_i)$ over the initial ketene thermal population $P(T_{beam},J_i)$ at a temperature of $T_{beam} = 4$ K, and over all allowed optical transitions. J_i signifies the i-th rotational level of the jet-cooled ground state ketene (corresponding to an energy of E_i) and $P(J,J_i)$ is the probability for a transition from J_i to J which is proportional to the Hönl−London factor. The signal can then be expressed by

$$S(v_{CO},J_{CO},h\nu) \propto \sum_i \sum_{J=J_i-1}^{J_i+1} \sigma(h\nu,E_i)P(J,J_i)P(T_{beam},J_i)\Phi(v_{CO},J_{CO},h\nu + E_i,J) \quad (4)$$

$$\approx \sigma(h\nu)\bar{\Phi}(v_{CO},J_{CO},h\nu)$$

where the $\sigma(h\nu,E_i)$ has been replaced by $\sigma(h\nu)$ based on the assumption that it is independent of the initial state of ketene. J_i specifies the ketene ground state angular momentum J, its molecular projections, K_a and K_c, and K_a in turn specifies the nuclear spin (*ortho* or *para*). The expression for $S(v_{CO},J_{CO},h\nu)$ implicitly includes a summation over K_a and the appropriate ΔK_a selection rules for the perpendicular optical transition.[24] Throughout the paper, a bar denotes an average as defined by eq 4.

The total quantum yield is the sum of the quantum yields for CO produced through the singlet and triplet channels, and eq 4 can be rewritten as

$$S(v_{CO},J_{CO},h\nu) = S_s(v_{CO},J_{CO},h\nu) + S_t(v_{CO},J_{CO},h\nu) \propto \sigma(h\nu)[\bar{\Phi}_s(v_{CO},J_{CO},h\nu) + \bar{\Phi}_t(v_{CO},J_{CO},h\nu)] \quad (5)$$

The experiment does not distinguish between CO produced through the singlet or triplet channel, so that $S(v_{CO},J_{CO},h\nu)$ is the measured quantity. Clearly, $S(1,J_{CO},h\nu) = S_t(1,J_{CO},h\nu)$ below the singlet threshold for the production of CO(v=1).

Using the averaged quantum yields an experimental rotational distribution probability for a given v_{CO} in the singlet channel can be defined as

$$P_e(J_{CO}|s,v_{CO}) = \frac{\bar{\Phi}_s(v_{CO},J_{CO},h\nu)}{\sum_{J'_{CO}} \bar{\Phi}_s(v_{CO},J'_{CO},h\nu)} = \frac{S_s(v_{CO},J_{CO},h\nu)}{\sum_{J'_{CO}} S_s(v_{CO},J'_{CO},h\nu)} \quad (6)$$

The fraction of CO formed in vibrational state v_{CO} is

$$P_e(v_{CO}|s) = \frac{\sum_{J'_{CO}} \bar{\Phi}_s(v_{CO},J'_{CO},h\nu)}{\sum_{v'_{CO},J'_{CO}} \bar{\Phi}_s(v'_{CO},J'_{CO},h\nu)} \quad (7)$$

and the singlet yield is

$$P_e(s) = \frac{\sum_{v'_{CO},J'_{CO}} \bar{\Phi}_s(v'_{CO},J'_{CO},h\nu)}{\sum_{v'_{CO},J'_{CO}} (\bar{\Phi}_s(v'_{CO},J'_{CO},h\nu) + \bar{\Phi}_t(v'_{CO},J'_{CO},h\nu))} \quad (8)$$

Since all excited ketene molecules dissociate, the denominator in eq 8 is equal to one. These conditional probabilities[3] are obtained directly from the experimental data,[32,33] so that the averaged quantum yield is

$$\bar{\Phi}_s(v_{CO},J_{CO},h\nu) = P_e(s)P_e(v_{CO}|s)P_e(J_{CO}|s,v_{CO}) \quad (9)$$

A. Vibrational Branching Ratios. For photon energies of 57, 110, 200, 357, and 490 cm^{-1} over the CO(v=1) threshold (2200, 2253, 2343, 2500, and 2633 cm^{-1} over the singlet threshold), vibrational branching ratios

$$\frac{P_e(1|s)}{P_e(0|s)} \equiv \frac{S_s(v_{CO}=1,h\nu)}{S_s(v_{CO}=0,h\nu)} \quad (10)$$

were measured (Table 1, Figure 2). These are the ratios of the

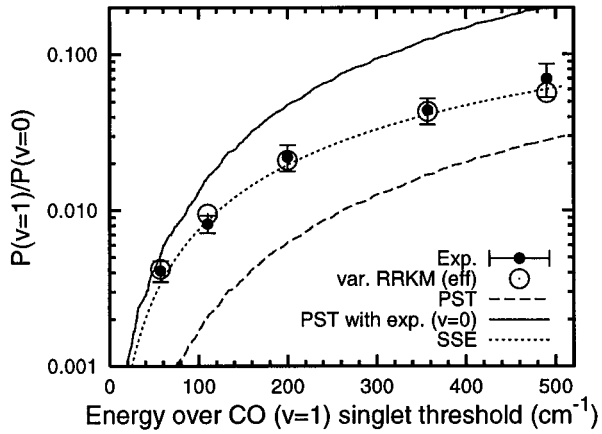

Figure 2. Singlet vibrational branching ratios. The solid circles are the experimental data. The error bars indicate 95% confidence intervals. The open circles represent the effective var. RRKM calculation.[14] The dashed line is PST. The solid line combines the PST rate for CO(v=1) with the measured rate for CO(v=0). The dotted line is the SSE prediction, eq 13.

averages over the thermally (4 K) populated states of ketene as experimentally measured.

A vibrational branching ratio can also be obtained for the triplet channel in this energy region:

$$\frac{P_e(1|t)}{P_e(0|t)} \equiv \frac{P_e(1|s)}{P_e(0|s)}\left\{\frac{S_t(h\nu,v_{CO}=1)}{S_s(h\nu,v_{CO}=1)}\right\}\left\{\frac{S_s(h\nu,v_{CO}=0)}{S_t(h\nu,v_{CO}=0)}\right\} \quad (11)$$

Here the bracketed ratios are the deconvoluted ratio of triplet signal intensity to singlet signal intensity in the rotational distributions measured in ref 32, in Table 2 and section III of that work. Values of $P_e(1|t)/P_e(0|t)$ are given in Table 1.

With $P_e(s)$ and $P_e(J_{CO}|s,v)$ taken from ref 32 and $P_e(v_{CO}|s)$ obtained from the vibrational branching ratios discussed above, the singlet quantum yields listed in Table 2 have been calculated. Using the triplet analog of eq 9, triplet quantum yields have also been calculated, with $P_e(t) = 1 - P_e(s)$, $P_e(v_{CO}|t)$ from Table 1 and $P_e(J_{CO}|t,v_{CO})$ set equal to the rotational distribution of CO slightly below the singlet channel threshold from ref 33. $\bar{\Phi}_t(v_{CO},J_{CO},h\nu)$ is nearly constant throughout the energy range studied (Table 2).

B. PHOFEX Spectra. Two series of PHOFEX spectra were measured on the CO A ← X (5 ← 1) Q branch, one for J_{CO} = 3 and one for J_{CO} = 7 (Figure 3). The PHOFEX curves rise sharply from the energy threshold for the production of the CO state being probed, then decline at higher energies as other CO rotational states become energetically accessible.[24] More product channels open as additional $^1CH_2$ states become energetically accessible in combination with the observed CO state, giving rise to the observed steps in the PHOFEX spectra. These steps match the energies of the $^1CH_2$ term values to within the experimental uncertainty of ±0.5 cm^{-1}.

The absorption cross section $\sigma(h\nu)$ of jet-cooled ketene has been assumed[24,29,30] to be independent of the photolysis energy. This assumption was tested by Garcia-Moreno *et al.*,[31] who found the cross section to be constant within 5% for the first

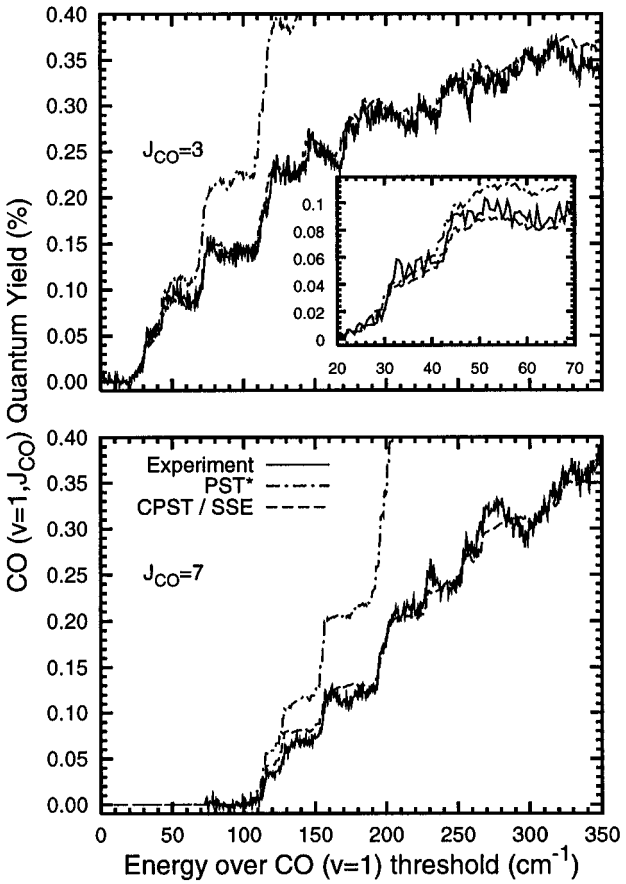

Figure 3. PHOFEX spectra for CO(v=1,J=3) and CO(v=1,J=7). The experimental PHOFEX spectra are placed on an absolute scale using the population distributions at 200 cm^{-1}. The calculated curves are on the same absolute scale, showing the quantum yield as a percentage of total yield. The dashed theoretical line is the yield when $P_e(J_{CO}|v,s)$ is given by PST constrained by the experimental $^1CH_2$ distributions (CPST), and $P_e(v|s)$ is given by SSE. The dash-dotted line is the yield when $P_e(J_{CO}|v,s)$ is given by PST and $P_e(v|s)$ is calculated by assuming that CO(v=1) follows PST while CO(v=0) follows experiment (PST*). The inset for CO(v=1,J=3) is given to show the first steps more clearly.

500 cm^{-1} over the singlet channel threshold, and within 10% up to 1000 cm^{-1} over the singlet channel threshold. At the much higher energies of this work, E > 2150 cm^{-1} over the singlet channel threshold, this assumption was tested in the same way. From eqs 4 and 5,

$$\sigma(h\nu) \propto \frac{S(v_{CO},J_{CO},h\nu) - S_t(v_{CO},J_{CO},h\nu)}{\bar{\Phi}_s(v_{CO},J_{CO},h\nu)} \quad (12)$$

Since $\bar{\Phi}_t(v_{CO},J_{CO},h\nu)$ is rather small and does not vary strongly with energy, $S_t(v_{CO},J_{CO},h\nu)$ can be set equal to its value just below the CO(v=1) singlet threshold channel. From the experimental values of $S(v_{CO},J_{CO},h\nu)$, $\sigma(h\nu)$ was calculated and normalized to its value σ_{200} at 200 cm^{-1} for each PHOFEX curve. As shown in Table 2, $\sigma(h\nu)/\sigma_{200}$ is constant to within ±0.05, except for CO(v=1,J=7) at 110 cm^{-1}, where it deviates by 0.08. Given the near constancy of $\sigma(h\nu)$, the PHOFEX

TABLE 2: Test for Dependence of PHOFEX on Triplet Quantum Yield and Dependence of Optical Cross Section on $h\nu$

excess energy[a]	triplet quantum yield (%)		singlet quantum yield (%)		$\sigma(h\nu)/\sigma_{200}$[b]	
	CO(v=1,J_{CO}=3)	CO(v=1,J_{CO}=7)	CO(v=1, $J_{CO=3}$)	CO(v=1,J_{CO}=7)	CO (v=1,J_{CO}=3)	CO (v=1,J_{CO}=7)
110	0.074 ± 0.017	0.19 ± 0.04	0.14 ± 0.02	0.009 ± 0.002	1.04	1.08
200	0.050 ± 0.011	0.13 ± 0.03	0.29 ± 0.04	0.18 ± 0.03	1.00	1.00
357	0.044 ± 0.023	0.11 ± 0.06	0.40 ± 0.06	0.38 ± 0.06	0.96	0.99

[a] As in Table 1. [b] See text.

spectra can be converted to absolute quantum yields using eq 12, with the absolute quantum yield from Table 2 at 200 cm^{-1} as the calibration point for each curve.

IV. Discussion

A. Singlet Channel Vibrational Branching Ratios. The experimental vibrational branching ratios are compared with the PST, separate statistical ensembles (SSE), and var. RRKM models in Table 1. PST severely underestimates the extent of vibrational excitation. Since PST is known to overestimate the singlet rate constant near 2500 cm^{-1},[10,33] a second approach is used in which the CO(v=1) rate constant is calculated from PST and the experimental CO(v=0) rate is used. This model (PST*) is appropriate for vibrationally adiabatic dynamics with a tightened transition state for the CO(v=0) surface and a completely loose transition state for CO(v=1). PST* should be exact at threshold; it overestimates the experimental branching ratio by a factor increasing from 25% at 57 cm^{-1} to a factor of 3 at 490 cm^{-1}. This indicates a modestly tightened transition state for energies as low as 57 cm^{-1}.

SSE, developed by Wittig and co-workers,[28] assumes PST rotational state distributions within each vibrational state, and assumes that $P_e(v_{CO}|s)$ is proportional to the density of states of an ensemble of the disappearing oscillators. For ketene in the energy range considered here (2200−2633 cm^{-1} over the singlet threshold),

$$P^{SSE}(v_{CO}) = \frac{(E - E_{v_{CO}})^{3/2}}{\sum_{v'}(E - E_{v'})^{3/2}} \qquad (13)$$

where v_{CO} gives the CO product vibrational state of interest and v' represents all possible combinations of product vibrational states for both products, which for this energy range are CO(v=0), CO(v=1), $^1CH_2$ (0,0,0), and $^1CH_2$ (0,1,0). For higher energies, a sum over accessible $^1CH_2$ states for each v_{CO} appears in the numerator. Although SSE contains no adjustable parameters, it predicts the vibrational distributions of $^1CH_2$[31] and the single vibrational branching ratio for CO determined at 357 cm^{-1} by Kim *et al.*[33] as accurately as does the more complex var. RRKM. SSE describes the vibrational branching ratio for CO(v=1)/CO(v=0) accurately for 110 $cm^{-1} \le E \le$ 490 cm^{-1} (Table 1, Figure 2). At 57 cm^{-1}, it underestimates the branching ratio by ∼20%. SSE does not account for the influence of the opening of individual rotational channels on the vibrational yields close to threshold.[31] Klippenstein and Allen have calculated the vibrational branching ratios from their *ab initio*-based var. RRKM[14] using eq 2. Figure 2 shows that both var. RRKM and SSE compare very well with experiment, thus confirming previous results[10,11,30,31] and indicating that the dynamics from transition state to fragments are vibrationally adiabatic for the CO stretch.

B. PHOFEX Spectra. The absolute quantum yields of CO(v=1,J=3,7) determined from the PHOFEX spectra are compared with two theoretical models in Figure 3. For the dash-dotted line, the yield is calculated using PST* as described above. For the dashed line, $P_e(v_{CO}|s)$ is assumed to follow SSE, and $P_e(J_{CO}|s,v_{CO})$ is calculated using PST constrained by the experimental $^1CH_2$ rotational distributions (CPST).[31,32] CPST predicts the rotational distributions of the CO(v=1) fragments well up to $E \le$ 500 cm^{-1}.[32]

This CPST/SSE model underestimates the yield at low energy, $E \le$ 70 cm^{-1}, but otherwise matches the experiment very well. Since SSE does not deal with the individual rotational channels of the loose transition state, it cannot be accurate at energies for which $P_e(v_{CO}|s)$ exhibits stepwise increases.[31]

The PST* model for CO(v=1) production gives the energetic position of the steps accurately but does not describe the amplitude well at all for $E \ge$ 40 cm^{-1}. This necessarily follows from the overestimate of the $P_e(v_{CO}=1|s)$ values in Figure 2 for $E \ge$ 57 cm^{-1}. For the CO(v=1,J=3) PHOFEX, this model does predict the first two steps, E<40 cm^{-1}, better than the CPST/SSE, which suggests that PST is accurate for $0 \le E \le$ 40 cm^{-1}.

C. Singlet Rate Constant. Rate constants may be obtained from the observed product quantum yields. Equation 3 defines the state-specific quantum yield for a particular rovibrational level of CO as proportional to the rate constant for production of that state. Equation 9 shows how the averaged singlet quantum yield can be obtained from experimental measurements. This averaged quantum yield is given in terms of rate constants by averaging both sides of eq 3:

$$\bar{\Phi}_s(v_{CO},J_{CO},h\nu) = \bar{k}_s(v_{CO},J_{CO},h\nu)/\bar{k}_{tot}(h\nu) \qquad (14)$$

The average of the ratio of rate constants on the right side of eq 3 can be approximated as the ratio of averaged rate constants because $k_{tot}(h\nu + E_i,J)$ does not vary significantly over the range of E_i or J. PST calculations at 2200 cm^{-1} over threshold give rate constants for $J = 0$ and for a ground state 4 K thermal average that differ by less than 1%.

Potter *et al.* have measured total rate constants for the dissociation of ketene from 450 to 6000 cm^{-1} over the singlet threshold.[35] These are used, along with the previously determined singlet yield,[32] to determine the singlet rate constants in this energy range. Rearranging eq 14, summing over all possible singlet product states, and combining that with eq 8 gives

$$\bar{k}_s(h\nu) = P_e(s)\bar{k}_{tot}(h\nu) \qquad (15)$$

where $\bar{k}_s(h\nu)$ and $\bar{k}_{tot}(h\nu)$ are the averaged singlet and total rate constants, respectively, and $P_e(s)$ is the singlet yield taken from ref 32. These rate constants are given in Table 3.

Below 450 cm^{-1}, there is no measured total rate constant, and $\bar{k}_s(h\nu)$ cannot be calculated by eq 15. However, the vibrational branching ratios and singlet rate constants just above the $^1CH_2$ + CO(v=1) threshold can be combined to give a singlet rate constant for production of CO(v=1), $\bar{k}_s(v_{CO}=1,h\nu)$. In the initial 500 cm^{-1} above the CO(v=1) threshold, the singlet rate constant is only available at a single energy, 2521 cm^{-1}, and a linear interpolation of log $\bar{k}_s(h\nu)$ is used for 2143−2643 cm^{-1} over threshold. The least-squares fit gives slope, 3.66 × 10^{-4} 1/cm^{-1}, and intercept, 9.01. The interpolated singlet rate constants and the vibrational branching ratios are then used to calculate a singlet rate constant for CO(v=1)

$$\bar{k}_s(v_{CO} = 1,h\nu) = P_e(1|s)\bar{k}_s(h\nu) \qquad (16)$$

The total rovibrational density of states, $\rho(h\nu + E_i,J)$, can be written as the vibrational density of states summed over the degenerate rotational states of the electronically excited ketene

$$\rho(h\nu + E_i,J) = \sum_{K=-J}^{K=J} \rho_v[h\nu + E_i - E(J,K)] \qquad (17)$$

Over the range of energies represented by E_i and $E(J,K)$, $\rho_v[h\nu + E_i - E(J,K)]$ is nearly constant and can be approximated by $\rho_v(h\nu)$, while the sum over K reduces to $2J + 1$. During the fragmentation of ketene, the nuclear spin state of the hydrogens, *ortho* or *para*, is conserved.[24] Thus, the statistical transition

TABLE 3: Rate Constants[a]

				log $\bar{k}_s(v=0)$				
							var. RRKM	
excess energy[b]	singlet yield[d]	log $\bar{k}_{tot}$[e]	log $\bar{k}_s(v_{CO}=1)$[e]	expt A[f]	expt B[f]	PST[g]	KEA 1[h,i]	KEA 2[h,i]
56	0.15 (0.03)		7.42 (0.11)		7.60 (0.11)	7.75	7.76	7.64
110	0.34 (0.03)		7.74 (0.10)		7.92 (0.10)	8.28	8.29	8.03
200			8.21 (0.09)		8.39 (0.09)	8.78	8.61	8.40
325	0.63 (0.04)		8.55 (0.09)		8.73 (0.09)	9.17	8.82	8.67
450[c]	0.71 (0.08)	9.04 (0.03)	8.80 (0.09)	8.89 (0.06)	8.98 (0.09)	9.45	8.97	8.83
1107	0.80 (0.05)	9.38 (0.07)		9.28 (0.08)		10.16	9.44	9.37
1435	0.86 (0.02)	9.59 (0.04)		9.52 (0.05)		10.4	9.58	9.52
1720	0.88 (0.02)	9.70 (0.10)		9.64 (0.10)		10.5	9.71	9.65
2521	0.92 (0.04)	10.00 (0.10)		9.96 (0.10)		10.8	9.99	9.93
2942	0.92 (0.04)	10.14 (0.08)		10.11 (0.09)		10.9	10.12	10.06
3217	0.92 (0.05)	10.18 (0.11)		10.14 (0.12)		11.0	10.21	10.15
3538	0.93 (0.05)	10.28 (0.04)		10.25 (0.06)		11.1	10.29	10.24
3763	0.91 (0.06)	10.25 (0.33)		10.21 (0.34)		11.1	10.35	10.30
4367	0.94 (0.05)	10.54 (0.07)		10.51 (0.09)		11.3	10.50	10.44
4870	0.94 (0.05)	10.66 (0.36)		10.63 (0.37)		11.5	10.60	10.55
4920	0.94 (0.05)	10.68 (0.28)		10.65 (0.29)		11.5	10.61	10.56
5598	0.92 (0.07)	10.75 (0.22)		10.71 (0.24)		11.7	10.74	10.69

[a] Numbers in parentheses give the 95% confidence intervals. [b] As in Table 1. [c] At this energy, the singlet yield was calculated at 490 cm^{-1} while the total rate constant was calculated at 450 cm^{-1}. [d] Singlet yield $P_e(s)$ defined in eq 8; the numbers and uncertainties are taken from ref 32. [e] Total rate constants taken from ref 35. [f] Expt A is calculated from the singlet yield and the total rate constant at the appropriate energy. log $\bar{k}_s(v_{CO}=1)$ is calculated from the singlet rate constant and the vibrational branching ratio at the appropriate energy. See the text for details. Expt B is calculated from log $\bar{k}_s(v_{CO}=1)$, adjusted for the correct density of states at 30 000 cm^{-1}. [g] From ref 10, using a total density of states of $\rho_{tot} = 0.94\rho_{DC}$. [h] From refs 13, 14, and 37 using a total density of states of $\rho_{tot} = 0.94\rho_{DC}$. [i] Calculated for $J' = 0$. The experimental and PST values are for a thermally populated ketene ground state at $T = 4$ K.

state theory of eq 1 must include only states of a single nuclear spin symmetry in $W(E, J)$ and $\rho(E, J)$. In the energy range for dissociation, the densities of *ortho* and *para* vibrational states by direct count are equal to within 0.5%, and

$$\rho_{ortho}(h\nu) = \rho_{para}(h\nu) = \rho_v(h\nu)/2 \qquad (18)$$

The +/− symmetry of ketene is also a conserved property,[7] but not one which can be resolved experimentally; thus, both $W(E, J)$ and $\rho(E, J)$ are summed over these two classes of states. The averaged singlet rate constant for nuclear spin state n can then be given by

$$\bar{k}_{s,n}(h\nu) = \sum_{v'_{CO},J'_{CO}} \bar{W}_{s,n}(v'_{CO},J'_{CO},h\nu)/h\rho_v(h\nu)/2 \qquad (19)$$

where

$$\bar{W}_{s,n}(v'_{CO},J'_{CO},h\nu) = \sum_i \sum_{J=J_i-1}^{J=J_i+1} P(J,J_i)P(T_{beam},J_i)\frac{W_{s,n}(v'_{CO},J'_{CO},h\nu + E_i,J)}{2J+1} \qquad (20)$$

The total singlet rate constant defined by averaging eq 3 as per eq 4 gives

$$\bar{k}_s(h\nu) = (3/4)\bar{k}_{s,ortho}(h\nu) + (1/4)\bar{k}_{s,para}(h\nu) \qquad (21)$$

since the statistical weights for *ortho* to *para* are 3 to 1.

Since the dissociation of ketene is vibrationally adiabatic, the CO frequency is nearly constant along the reaction coordinate[13] and the rotational constant of CO changes very little with v_{CO}, $W_{s,n}(v_{CO},J_{CO},h\nu+E_i)$ is a function of excess energy, so that

$$W_{s,n}(v_{CO} = 0, J_{CO}, h\nu + E_i, J) = W_{s,n}(v_{CO} = 1, J_{CO}, h\nu + E_i + 2143.2\ cm^{-1}, J) \qquad (22)$$

Nonetheless, the rate constants for $v_{CO} = 1$ and $v_{CO} = 0$ at a given energy above their respective thresholds are expected to differ because the total rovibrational density of states is a function of the absolute energy. To calculate $\bar{k}_s(v_{CO}=0,h\nu)$, the density of states is assumed to be proportional to the anharmonic direct count density of states, ρ_{DC}, reported by East *et al.*[20] for a complete *ab initio* anharmonic vibrational analysis of ketene (model 3 of ref 13). Therefore, the rate constants for $v_{CO} = 1$ and $v_{CO} = 0$ can be related using eqs 19 and 22,

$$\bar{k}_s(v_{CO} = 1, h\nu + 2143.2\ cm^{-1}) = \bar{k}_s(v_{CO} = 0, h\nu)\frac{\rho_{DC}(h\nu)}{\rho_{DC}(h\nu + 2143.2\ cm^{-1})} \qquad (23)$$

This direct count gives a vibrational density of states of 1.99×10^4 1/cm^{-1} at 30 000 cm^{-1} and 3.12×10^4 1/cm^{-1} at 32 000 cm^{-1}, about 6% and 8% larger than the corresponding Whitten−Rabinovich values of 1.89×10^4 1/cm^{-1} at 30 000 cm^{-1} and 2.88×10^4 1/cm^{-1} at 32 000 cm^{-1}.[6] A harmonic direct count density of states yields values that are 5% and 3% lower than the Whitten−Rabinovich values, giving 1.80×10^4 1/cm^{-1} at 30 000 cm^{-1} and 2.77×10^4 1/cm^{-1} at 32 000 cm^{-1}. Using the anharmonic ρ_{DC}, $\bar{k}_s(v_{CO}=0,h\nu)$ is therefore expected to be 54% larger than $\bar{k}_s(v_{CO}=1,h\nu+2143.2\ cm^{-1})$, near their respective thresholds. The singlet rate constants, $\bar{k}_s(v_{CO}=1,h\nu)$ and $\bar{k}_s(v_{CO}=0,h\nu)$, for $E \le 500\ cm^{-1}$, are given in Table 3. $\bar{k}_s(v_{CO}=0,h\nu)$ for 57 $cm^{-1} \le E \le 6000\ cm^{-1}$ is shown in Figure 4. Below 2143 cm^{-1}, of course, $\bar{k}_s(v_{CO}=0,h\nu)$ is identical to $\bar{k}_s(h\nu)$, since no CO(v=1) can be produced. At 490 cm^{-1}, the singlet rate constant $\bar{k}_s(v_{CO}=0,h\nu)$ can be calculated directly from the total rate constant and singlet yield[32] or from the v_{CO}=1 data. The two values of log $\bar{k}_s(v_{CO}=0,h\nu)$, 8.89(0.07) and 8.98(0.09), agree quite closely and confirm the validity of eqs 16 and 23.

PHOFEX spectra can be used to calculate the rate as a continuous function of energy (eqs 6−8, 14, 15 and 16).

$$\bar{k}_s(v_{CO}=1,h\nu) = \frac{\bar{\Phi}_s(v_{CO}=1,J_{CO},h\nu)\bar{k}_{tot}(h\nu)}{P_e(J_{CO}|s,v_{CO}=1)} \propto \frac{S_s(v_{CO}=1,J_{CO},h\nu)\bar{k}_{tot}(h\nu)}{P_e(J_{CO}|s,v_{CO}=1)} \qquad (24)$$

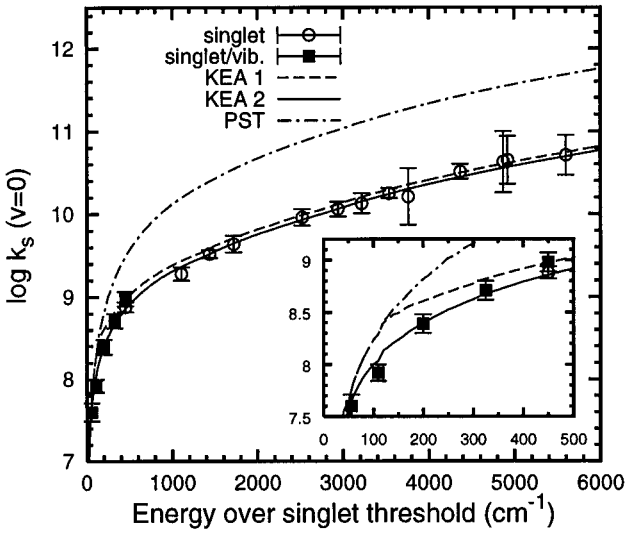

Figure 4. Singlet rate constants. The open circles are the points for the singlet rate constant calculated from the singlet yield (ref 32) and the total rate constant. The solid squares are from the experimental values of the rate constants for CO(v=1) production, the vibrational branching ratio at E, and the ratio of the direct count density of states near 32 500 and 30 000 cm^{-1} (see text). The dot-dashed line is the PST rate constant. The dashed line is the KEA1 var. RRKM calculation, and the solid line is the KEA2 var. RRKM calculation, ref 13. See the text for a description of these calculations. The inset shows an expanded version of this figure, up to 500 cm^{-1}.

$S_s(h\nu,v_{CO}=1,J_{CO})$ is measured every 0.5 cm^{-1}. The smooth interpolation above for $\bar{k}_s(h\nu)$ is used for $\bar{k}_{tot}(h\nu)$. The experimentally determined rotational distributions are described well by PST up to 200 cm^{-1} and by CPST up to 500 cm^{-1} over the singlet channel CO(v=1) threshold;[32] the detailed structure in $P_e(J_{CO}|s,v_{CO}=1)$ is given by these calculations.[32] Rate constants were calculated from the Q(3) and Q(7) spectra, as well as from a previously reported PHOFEX spectrum for $^1CH_2$ $(0,1,0)1_{01}$.[31] The latter was used only up to 200 cm^{-1}, the highest energy at which the rotational distribution is given accurately by PST. The proportionality constant, eq 24, for all three PHOFEX spectra was set to match the experimental rate at 200 cm^{-1}, and the results were averaged to give the experimental rate in Figure 5. Below 30 cm^{-1}, only the $^1CH_2$ data is used, and the overall rate constant is then solely given by $\bar{k}_{s,ortho}(h\nu)$.

D. Models for the Singlet Rate Constant. The PST, var. RRKM,[10,13] and SACM[15,16] models mentioned in the introduction are used to calculate W in eqs 19−20 for comparison to experiment. In all models the rate constant must approach the PST limit at threshold. There are no adjustable parameters in the calculation of W_{PST} shown in Figure 5. The corresponding PST rate constant, Figures 4 and 5, increases much more rapidly with energy than the experimental values of $k_s(v_{CO}=1,h\nu)$. The transition state begins to tighten at 35 ± 5 cm^{-1}. However, for E < 30 cm^{-1} above the v = 1 threshold, W_{PST} parallels the observed rate in all of its details including the steps at 15 and 21 cm^{-1}. This allows an "experimental" density of states to be derived from eq 19. The result of (3.35 ± 0.33) × 10^4 1/cm^{-1} at 32 259 cm^{-1} is 1.01 ± 0.11 times the *ab initio* direct count of Klippenstein, Allen, and East,[13] 1.16 ± 0.13 times the harmonic direct count, and 1.10 ± 0.12 times the Whitten−Rabinovich estimate, all well within the experimental and computational uncertainties.

RRKM fits of the rate constant for the dissociation of ketene along the triplet channel determined the density of states for ketene near 28,250 cm^{-1} to be 1.07 g_t times the *ab initio* density of states (1.11g_t times the Whitten-Rabinovich density), where

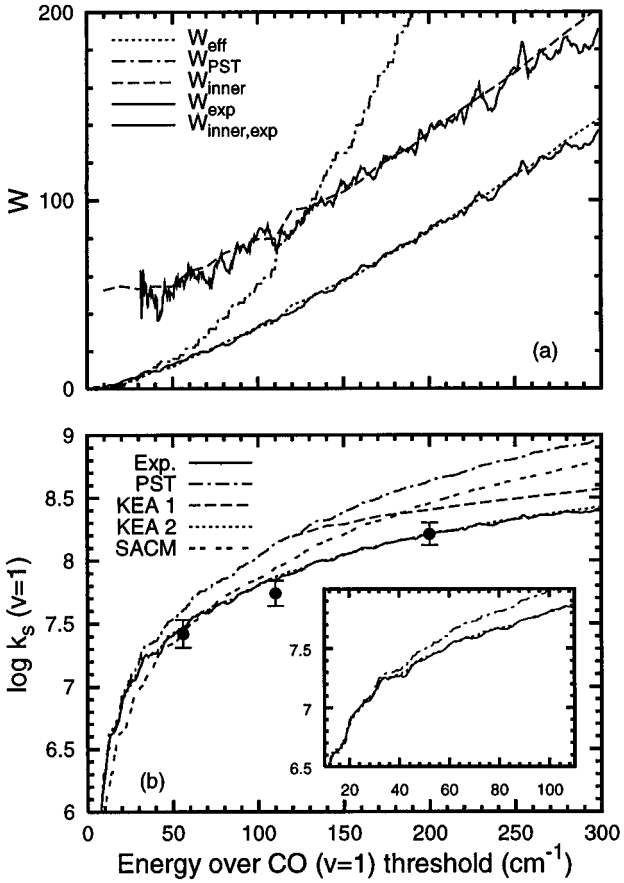

Figure 5. (a) Number of open channels for tight and loose transition states. The dot-dashed line is $\bar{W}_{PST}(h\nu)$, for a PST transition state under the conditions of the experimental data shown in (b). The dashed line is $\bar{W}_{inner}(h\nu)$, taken from refs 13, 14, and 37, for a tight transition state with a C−C bond between 2.1 and 3.1 Å. The dotted line is $\bar{W}_{eff}(h\nu)$, as described in eq 2 in the text. The lower solid line is $\bar{W}_{exp}(h\nu)$, the experimental number of open channels, and the upper solid line is an experimental value of $\bar{W}_{inner}(h\nu)$, calculated by treating $\bar{W}_{exp}(h\nu)$ as the effective number of open channels in eq 2 and using $\rho_v(h\nu) = 0.94\rho_{DC}$ as density of states. (b) Singlet channel rate constant from PHOFEX data at low energy. The solid line is the continuous experimental rate constant from the PHOFEX data. The solid circles are the experimental rate constants derived from the singlet rate at ∼2500 cm^{-1} and the vibrational branching ratios. The dot-dashed line is the PST rate constant. The double-dashed line is an SACM rate constant, calculated with $\alpha/\beta = 0.6$, the dashed line is the KEA1 var. RRKM calculation, and the dotted line (nearly coincident with the experimental rate) is the KEA2 var. RRKM calculation. The inset shows more clearly the region where PST begins to fail. Only PST, KEA2, and the experimental lines are shown.

g_t is the number of strongly coupled triplet levels.[36] The experimental density of states above implies that g_t = 1.0 ± 0.1.

Var. RRKM calculations of W_{inner} (Figure 5) by Klippenstein, Allen, and co-workers[13,37] are based on high-level *ab initio* calculations of the potential energy surface and reaction coordinate for singlet ketene. Although some significant choices of calculational method were necessary, it is important to note they were made before our near-threshold rate data were available and that there are no adjustable parameters in the calculation. The values are an unweighted sum of W_{inner} for *ortho* and *para* with $J = 0$. In the range of 80−300 cm^{-1}, the difference in W_{PST} between *ortho* and *para* is less than 20% and decreases with increasing energy. W_{inner} should exhibit much smaller differences. Likewise, the impact of using J = 0 should affect the calculated rate constants by less than 5%. Above 1000 cm^{-1}, the rate constant calculated from W_{inner}

coincides well with experiment (Figure 4). For the standard var. RRKM (KEA1), $W(h\nu)$ in eq 1 is the minimum number of available states, at any point along the reaction coordinate. $W_{PST} = W_{inner}$ at 130 cm^{-1}. This is the switching point between control by the outer and inner transition states. The calculated rate constant is larger than experiment between 40 and about 1000 cm^{-1}, but close on either end of this range. The unified statistical model of eq 2 (KEA2) fits the data to within 25% over the entire 6000 cm^{-1} range when W_{max} is assumed to be large enough to be negligible. The density of states which gives the best fit between experiment and KEA2 is $\rho_\nu(h\nu) = 0.94\rho_{DC}$, identical to the *ab initio* value to well within the experimental and computational uncertainties. This excellent agreement between experiment and KEA2 is also evident in the number of open channels shown in Figure 5. In addition to $\bar{W}_{eff}$ and $\bar{W}_{PST}$, the figure also shows an "experimental" value $\bar{W}_{exp}$, calculated from the continuous rate constant between 10 and 300 cm^{-1} using eq 19 with $\rho_v(h\nu) = 0.94\rho_{DC}$. Clearly, $\bar{W}_{inner}(h\nu)$ is much larger than $\bar{W}_{exp}(h\nu)$ over this energy region, while $\bar{W}_{eff}(h\nu)$ is within a few percent of $\bar{W}_{exp}(h\nu)$. Additionally, an "experimental" value $\bar{W}_{exp,inner}(h\nu)$ of the number of channels at the inner transition state is calculated for 40 $cm^{-1} < E <$ 300 cm^{-1},

$$\frac{1}{\bar{W}_{exp,inner}(h\nu)} = \frac{1}{\bar{W}_{exp}(h\nu)} - \frac{1}{\bar{W}_{PST}(h\nu)} \qquad (25)$$

$\bar{W}_{exp,inner}(h\nu)$ is also shown in Figure 5 and is nearly equal to the value of $\bar{W}_{inner}(h\nu)$ calculated by Klippenstein *et al.*[13] This is a truly remarkable agreement between a completely *ab initio* theory and an experimental rate constant and provides strong support for the validity of the unified statistical model.[18]

A key assumption in the unified statistical model is that energy is randomized between the inner and PST transition states. A molecule coming through the inner transition state on a particular adiabatic channel must undergo a sufficient number of nonadiabatic transitions between curves so that all W_{max} channels are statistically represented before the molecule approaches the PST transition state. In the range 40 $< E <$ 200 cm^{-1}, the observed rate constant is clearly less than the PST value whereas the product energy state distributions are given accurately by PST.[31,32] This indicates that full randomization of energy occurs between transition states. The fact that the dipolar attraction at long range orients the methylene carbon away from the carbonyl carbon to which it bonds[13] may be important in this energy redistribution and may limit the applicability of these results to other systems. For $E >$ 200 cm^{-1}, CH_2 rotational distributions become colder than statistical[31] and the energy randomization hypothesis must begin to break down. At 300 cm^{-1}, where W_{PST} is 3 times larger than W_{inner}, the observed rotational populations deviate from PST by some 35% on average. It is also expected that W_{max}/W_{PST} approaches unity and that both become much larger than W_{inner} as the total energy becomes large compared to the dipolar and dispersion energies of attraction.

For a truly complete *ab initio* test of the unified statistical model against the ketene data, W_{max} needs to be calculated. It may also be necessary to calculate W_{inner} near threshold for somewhat larger values of the reaction coordinate. The explicit inclusion of W_{max} would cause W_{eff} to approach W_{inner} somewhat more quickly as energy increases. This in turn would give a slightly larger density of states, closer to the $(1.01 \pm 0.11)\rho_{DC}$ determined from the first two steps in the rate constant. However, these additional refinements seem unlikely to produce changes of more than 10−20% in W_{eff} in the 50−300 cm^{-1} energy range of key interest.

Rate constants were calculated using the most approximate form of SACM introduced by Troe[15,16] for a simple Morse attractive potential with a dependence on fragment rotational angle. For this model, the parameter α/β controls the angular anisotropy of the potential and consequently how rapidly the energy level spacings increase as the chemical bond forms. For $\alpha/\beta = 1$, SACM and PST are identical; for $\alpha/\beta = 0$, SACM is equivalent to RRKM for a rigid transition state. Much thermal data for reactions without barriers can be fit with $\alpha/\beta \approx 0.5$.[16] The potential uses the same angular dependence for loose transition states as for the tight transition state important in the thermal data. Since angles are likely to be much more tightly defined where bonds are nearly formed than at long range, this is a poor form of potential for treating the energy region through which transition state tightening occurs. However, this is the only SACM model for which quantitative calculations have been possible. Consequently, this model should not be expected to, and does not, fit the ketene data near threshold (Figure 5). If smaller values of α/β are chosen to fit the rate at higher energy, the rate near threshold is calculated to be much smaller than observed. The form of the model potential cannot reproduce the data. For noncrossing adiabatic channels and strictly adiabatic dynamics, SACM must give the same rate constant as does the standard var. RRKM for the identical potential. Of course, for the adiabaticity assumed in this simplest SACM, the energy randomization required between the inner and PST transition states in the unified statistical model is not possible. Thus, a strictly adiabatic SACM with the *ab initio* potential produces the curve KEA1 and not the fit of KEA2. Maergoiz, Nikitin, and Troe[21,22] have shown the importance of narrowly avoided crossings between adiabatic curves and added this to the SACM. This provides a framework for a dynamical theory which could give both rate constants and product energy distributions. Such a detailed approach may be necessary for rates and especially product energy state distributions in situations which are between the complete energy randomization hypothesis of the unified statistical model and completely adiabatic models for dynamics between the inner transition state and the separated fragments.

E. Triplet Vibrational Branching Ratio. For the triplet channel, unlike the singlet channel, there is no quantitative theoretical model for calculation of the vibrational branching ratio determined in section III.A and given in Table 1. If the dynamics are assumed to be vibrationally adiabatic in the repulsive exit valley of the triplet surface, the triplet rate constants determined in ref 33 may be used to estimate a branching ratio using the triplet analogs of eqs 7, 14, and 23:

$$\frac{P_e(1|t)}{P_e(0|t)} = \frac{\bar{k}_t(h\nu - h\nu_2)}{\bar{k}_t(h\nu)} \frac{\rho_\nu(h\nu - h\nu_2)}{\rho_\nu(h\nu)} \qquad (26)$$

Here ν_2 is the frequency of the CO stretch at the transition state. This equation is valid only if the triplet channel dynamics are vibrationally adiabatic. For the triplet transition state, ν_2 is taken from Allen and Schaefer;[38] it is 1878 cm^{-1} for the C_s^I transition state and 1841 cm^{-1} for the C_s^{II} transition state. At energies just over the singlet threshold for production of CO(υ=1), log $\bar{k}_t(h\nu)$ is 8.83 ± 0.10, as interpolated from Table 3. At 1850 cm^{-1} below that energy, log $\bar{k}_t(h\nu)$ is 8.5 ± 0.1. This gives a value of 0.47 ± 0.09 for $P_e(1|t)/P_e(0|t)$ if the dynamics are adiabatic in the CO stretch. This is about 8 times larger than the measured value. If ν_2 is taken to be 2143.2 cm^{-1}, the vibrational frequency of free CO, log $\bar{k}_t(h\nu)$ is 8.4 ± 0.1, and the predicted vibrational branching ratio is 0.37 ± 0.07. If the triplet channel were vibrationally adiabatic, then the triplet yield

of CO(v=1) would have been comparable to, rather than much less than, the singlet yield. These results indicate that CO vibrational excitation at the transition state relaxes in the exit channel of the triplet PES.

V. Conclusions

The major result of this paper is the quantitative agreement between the experimental dissociation rate constant for ketene and that calculated completely *ab initio* for the unified statistical model of eq 2. The rate is studied with half-wavenumber resolution near threshold and measured up to a total energy of 6000 cm^{-1}. The results constitute striking support for this model of dissociation on the S_0 potential energy surface without a barrier to recombination. The observed rate exhibits no knee that would suggest sudden switching from an outer to an inner transition state. For energies between 40 and at least several hundred cm^{-1}, the reactive flux must be controlled by an inner transition state near 3 Å and a completely loose transition state acting in series. The unified statistical model assumption of energy randomization between the two transition states is experimentally verified up to 200 cm^{-1} but begins to break down at higher energies. The van der Waals and dipolar attractive forces between CH_2 and CO are sufficient at long range to produce a significant increase in density of states inside the PST transition state. It seems likely that this is a general feature of all dissociations without a barrier to recombination. The reaction is vibrationally adiabatic with respect to product vibrations with transition states defined separately for each vibrationally adiabatic potential energy surface. The results are a striking demonstration of the power of *ab initio* quantum chemistry and transition state theory.

The *ab initio* full anharmonic direct count density of states is within a few percent of the harmonic direct count, the Whitten−Rabinovitch approximation, and the density which gives the best fit of eq 2 to the observed rates. This stands in contrast to the spectroscopically measured densities of states at the dissociation limits of H_2CO, HCCH, and HFCO which all exhibit densities of states roughly 5 times those calculated.[3,25] Can we generally expect that larger molecules with less average excitation per oscillator will exhibit densities of states in line with expectations?

The observed density of states shows that for the triplet state dissociation reaction only one of the three triplet spin sublevels of ketene is active in the reaction process. In contrast to the singlet reaction channel, vibrational excitation of CO is found to relax as it moves from the transition state through the repulsive exit valley on the triplet potential energy surface.

Acknowledgment. This work was supported by the Chemical Sciences Division of the U.S. Department of Energy under Contract No. DE-AC03-76SF00098. A.M. also thanks the Deutsche Forschungsgemeinschaft for a postdoctoral fellowship. M.A.H. thanks the National Science Foundation for a graduate research fellowship. C.B.M. thanks the Alexander von Humboldt-Stiftung for a research award and Professor Jürgen Troe for his hospitality and many discussions of ketene dynamics. The authors thank Professors Stephen Klippenstein and Wesley Allen for many helpful discussions and for providing early access to new var. RRKM rate constants, Michael V. Ashikhmin for access to his direct count program, and Douglas Wade for providing many hours of computer programming assistance.

References and Notes

(1) Gilbert, R. G.; Smith, S. C. *Theory of Unimolecular and Recombination Reactions*; Blackwell Scientific: Oxford, U.K., 1990.
(2) Reisler, H.; Wittig, C. *Annu. Rev. Phys. Chem.* **1986**, *37*, 307.
(3) Green, W. H.; Moore, C. B.; Polik, W. F. *Annu. Rev. Phys. Chem.* **1992**, *43*, 591.
(4) Moore, C. B.; Smith, I. W. M. *J. Phys. Chem.* **1996**, *100*, 12848.
(5) Baer, T.; Hase, W. L. *Unimolecular Reaction Dynamics: Theory and Experiments*; Oxford University Press: Oxford, U.K., 1996.
(6) Holbrook, K. A.; Pilling, M. J.; Robertson, S. H. *Unimolecular Reactions*, 2nd ed.; Wiley: New York, 1996.
(7) Pechukas, P.; Light, J. C. *J. Chem. Phys.* **1965**, *42*, 3281.
(8) Marcus, R. A. *J. Chem. Phys.* **1986**, *85*, 5035; *Chem. Phys. Lett.* **1988**, 144, 208. Wardlaw, D. M.; Marcus, R. A. *Adv. Chem. Phys.* **1988**, 70, 231.
(9) Klippenstein, S. J.; Khundkar, L. R.; Zewail, A. H.; Marcus, R. A. *J. Chem. Phys.* **1988**, *89*, 4761.
(10) Klippenstein, S. J.; Marcus, R. A. *J. Chem. Phys.* **1989**, *91*, 2280.
(11) Klippenstein, S. J.; Marcus, R. A. *J. Chem. Phys.* **1990**, *93*, 2418.
(12) Yu, J.; Klippenstein, S. J. *J. Phys. Chem.* **1991**, *95*, 9882.
(13) Klippenstein, S. J.; East, A. L. L.; Allen, W. D. *J. Chem. Phys.* **1996**, *105*, 118.
(14) Klippenstein, S. J.; Allen, W. D. *Ber. Bunsenges. Phys. Chem.* **1997**, *101*, 423−437.
(15) Quack, M.; Troe, J. *Ber. Bunsenges. Phys. Chem.* **1974**, *78*, 240.
(16) Troe, J. *J. Chem. Phys.* **1981**, *75*, 226.
(17) Katagiri, H.; Kato, S. *J. Chem. Phys.* **1993**, *99*, 8805.
(18) Miller, W. H. *J. Chem. Phys.* **1976**, *65*, 2216−2223.
(19) Miller, W. H. In *Potential Energy Surfaces and Dynamics Calculations*; Truhlar, D. G., Ed.; Plenum: New York, 1981; pp 265−286.
(20) East, A. L. L.; Allen, W. D.; Klippenstein, S. J. *J. Chem. Phys.* **1995**, *102*, 8506.
(21) Maergoiz, A. I.; Nikitin, E. E.; Troe, J. *J. Chem. Phys.* **1991**, *95*, 5117.
(22) Maergoiz, A. I.; Nikitin, E. E.; Troe, J.; Ushakov, V. G. *J. Chem. Phys.* **1996**, *105*, 6263, 6270, 6277.
(23) Truhlar, D. G.; Garrett, B. C.; Klippenstein, S. J. *J. Phys. Chem.* **1996**, *100*, 12771.
(24) Chen, I. C.; Green, W. H.; Moore, C. B. *J. Chem. Phys.* **1988**, *89*, 314.
(25) Miyawaki, J.; Yamanouchi, K.; Tsuchiya, S. *Chem. Phys. Lett.* **1991**, *180*, 287.
(26) Ionov, S. I.; Davis, H. F.; Mykhaylichenko, K.; Valachovic, L.; Beaudet, R. A.; Wittig, C. *J. Chem. Phys.* **1994**, *101*, 4809. Abel, B.; Hamann, H. H.; Lange, N. *Faraday Discuss. Chem. Soc.* **1995**, *102*, 147. Jost, R.; Nygard, J.; Pasinski, A.; Delon, A. *J. Chem. Phys.* **1996**, *105*, 1287.
(27) Qian, C. X. W.; Ogai, A.; Reisler, H.; Wittig, C. *J. Chem. Phys.* **1989**, *90*, 209.
(28) Wittig, C.; Nadler, I.; Reisler, H.; Catanzarite, J.; Radhakrishnan, G. *J. Chem. Phys.* **1985**, *83*, 5581.
(29) Green, W. H.; Chen, I. C.; Moore, C. B. *Ber. Bunsenges. Phys. Chem.* **1988**, *92*, 389.
(30) Green, W. H.; Mahoney, A. H.; Zheng, Q.-K.; Moore, C. B. *J. Chem. Phys.* **1991**, *94*, 1961.
(31) Garcia-Moreno, I.; Lovejoy, E. R.; Moore, C. B. *J. Chem. Phys.* **1994**, *100*, 8890, 8902.
(32) Wade, E. A.; Clauberg, H.; Kim, S. K.; Mellinger, A.; Moore, C. B. *J. Phys. Chem.* **1997**, *101*, 732.
(33) Kim, S. K.; Choi, Y. S.; Pibel, C. D.; Zheng, Q.-K.; Moore, C. B. *J. Chem. Phys.* **1991**, *94*, 1954.
(34) Hirschfelder, J. O.; Wigner, E. *J. Chem. Phys.* **1939**, *7*, 616−628.
(35) Potter, E. D.; Gruebele, M.; Khundkar, L. R.; Zewail, A. H. *Chem. Phys. Lett.* **1989**, *164*, 463.
(36) Kim, S. K.; Lovejoy, E. R.; Moore, C. B. *J. Chem. Phys.* **1995**, *102*, 3218.
(37) Klippenstein, S. J., private communication.
(38) Allen, W. D.; Schaefer, H. F., III. *J. Chem. Phys.* **1986**, *84*, 2212.